19th Brazilian Congress of Thermal Sciences and Engineering
November 6th–10th, 2022, Bento Gonçalves - RS - Brazil

ENC-2022-0442
Solution of Transonic Flow Over a Supercritical Wing With Forced Oscillation

Pedro Vinícius Souza Coimbra
Henrique Matos Campos
Aluisio Viais Pantaleão
Department of Mechanical Engineering, School of Engineering, São Paulo State University (Unesp), Brazil
pedro.vs.coimbra@unesp.br, henrique.campos@unesp.br, aluisio.pantaleao@unesp.br

The fundamental challenge in computational aeroelasticity is providing accurate data on the behavior of aerodynamic forces when coupled with flexible structures. This work aims to develop a numerical methodology to solve transonic flows over wings with forced oscillation using only open-source software. To accomplish our goal, we analyzed the test case 3B from the AePW-2 workshop, doing the preprocessing and mesh generation in Salome Platform and the numerical solution in SU2. The selected test case consisted of the Benchmark Supercritical Wing (BSCW) in a forced oscillation with a frequency of 10 Hz and 1° of amplitude. In the studied case, the Mach number was 0.85, and the angle of attack (AOA) was 5°. Since the analyzed flow is considered turbulent, we used the RANS equations and the SA turbulence model to model the turbulence. We validated our methodology by doing the Grid Convergence Index (GCI) analysis, considering a steady-state flow and the wing stationary being the convergence achieved between the fine and the medium mesh with a GCI of 2.2%. The results obtained presented good agreement with the experimental data.

Keywords: *CFD, Transonic Flows, Open-Source Software, SU2, AePW-2,*

1. INTRODUCTION

Aeroelasticity is the subject that describes the interaction of aerodynamic, inertia, and elastic forces for a flexible structure and the phenomena that can result from it (Bisplinghoff *et al.*, 2013). One of the most relevant phenomena related to aeroelasticity is the flutter which influences structural stability and can cause catastrophic failures. The computation of the accurate pressure coefficient is vital for reliable aeroelasticity predictions, being the aerodynamics studies responsible for providing these coefficients.

Many aircraft operate in the transonic flow regime, and due to that, it is important to predict the flow behavior in this condition. However, this flow regime is complex due to the appearance of highly non-linear phenomena that can trigger flow separation, moving shock waves, and natural unsteadiness, as presented by Begnini *et al.* (2016).

Understanding aeroelasticity and transonic flows are vital in aircraft design, and that is why the National Aeronautics and Space Administration (NASA) aims to bring innovation to this field with the Aeroelastic Perdition Workshop (AePW). This workshop is organized to assess the state-of-the-art computational methods for predicting unsteady flow fields and aeroelastic responses. The goals are to provide an impartial forum to evaluate the effectiveness of existing computer codes and modeling techniques and identify computational and experimental areas needing additional research and development.

In the first Aeroelastic Prediction Workshop three geometries were studied, the Rectangular Supercritical Wing (RSW), the Benchmark Supercritical Wing (BSCW), and the High Reynolds Number Aero-Structural Dynamics (HIRENASD) wind tunnel model. The RSW case was supposed to be the case with lower complexity, nevertheless, according to Heeg (2013), the mounting system increased the case difficulty because the splitter plate was undersized and close to the wall, causing the tunnel wall boundary layer to affect the flow over the wing. Due to that, the efforts were changed to the BSCW. Heeg (2013) documented that many research groups had difficulty achieving a converged solution for this case configuration. The challenges of analyzing the BSCW model stem from the flow physics acting on the wing for the conditions studied. Initially, the difficulty was associated only with a shock induced detached flow, however, Heeg and Piatak (2013) showed through data analysis that this case contains an oscillatory shock. The HIRENASD case is well documented in the literature (Ballmann *et al.* (2011), Ballmann (2008), Chwalowski *et al.* (2011)). In the test case studied for the AePW, this wing does not appear to have a separated flow. The numerical and experimental analyses were in better agreement for the HIRENASD configuration than for the simpler planforms.

In the second edition of AePW (AePW-2), experimental data for the Benchmark Supercritical Wing (BSCW) were provided, including wing configurations for static, forced oscillation, and flutter conditions. The fundamental challenge in

computational aeroelasticity is providing accurate data on the behavior of aerodynamic forces when coupled with flexible structures, as detailed by Heeg *et al.* (2015).

The data provided in the AePW-2 covers three different cases, summarized in Table 1. The solution of all the cases, until now, was done only by Begnini *et al.* (2016) and Raveh *et al.* (2018).

Table 1. Cases of the second AePW, as presented by Heeg *et al.* (2015)

	Case 1	**Case 2**	**Optional Case 3A**	**Optional Case 3B**	**Optional Case 3C**
Mach	0.7	0.74	0.85	0.85	0.85
AoA	3°	0°	5°	5°	5°
Dynamic Data Type	Forced Oscillation f = 10Hz, |θ|=1°	Flutter	Unforced Unsteady	Forced Oscillation f = 10Hz, |θ|=1°	Flutter

In Begnini *et al.* (2016), the authors used CFD and AIC-Based methods to solve the AePW-2 cases. For the CFD analysis, the tools used were CFD++ and CMSoft Aero. Both CFD codes showed similar results for case 1, while case 3B was only analyzed with CFD++. The results were also compatible with experimental data, except in the region after the shock wave, where the pressure coefficient obtained was lower. On the other hand, to solve case 2, the authors used AIC-Based methods with the tools MSC/Nastran and ZAERO. The results obtained for this methodology ranged from 10% to 20% with the classical Doublet-Lattice Method (DLM) and for a more elaborated DLM, the results were about 5% conservative. Raveh *et al.* (2018) used an in-house multi-zone Euler/Navier-Stokes code, named EZNSS. Their results showed good agreement with experimental data for cases 1 and 2, however, in case 3 none of the turbulence models applied, SST or SA could capture the pressure recovery behind the shock wave.

In Campos et al. (2021), the authors solved cases 1 and 3A using the SU2 software. They used Ansys Mesh to discretize the domain. Their results showed good agreement with experimental data. Except for the shock region in case 3A, where the mesh was likely, not refined enough, the mesh used for case 3A had only 1.7 M elements.

As presented by Campos *et al.* (2021), in-house and commercial codes have limitations in the context of research within academia. As an alternative, Open-source software can be used, being two of the most relevant SU2 and OpenFOAM. Nevertheless, the former was built with a compressible approach, as shown by Economon *et al.* (2016), and has great potential in solving transonic flows.

The SU2 capabilities for solving complex flows have already been demonstrated in the literature. In Palacios *et al.* (2014), the authors studied the flow over RAE 2822 airfoil, Onera M6 wing, and the DLR-F6 aircraft, the study showed good agreement with experimental data for all cases. Sanchez *et al.* (2016) demonstrated the Fluid Structure Interaction (FSI) capabilities of SU2 by presenting results in good agreement with the literature.

This work aims to solve Case 3B, which has not been solved using an open-source solver to date. This is one of the most complex cases from the workshop due to a combination of forced oscillation, detached flow and moving shock waves. It will be simulated in SU2 with the mesh generated in Salome Platform.

2. THEORETICAL BACKGROUND

2.1 Governing Equations

According to Heeg *et al.* (2015), test case 3B consists of a transonic flow problem, the flow was assumed as turbulent and compressible. Since the test case analyzed an R-134a fluid flow, AePW-2 considered the fluid as Newtonian and isotropic. Given these assumptions, to evaluate the flow field, we needed to solve the conservation equations for mass, momentum, and energy, respectively, 1, 2, and 3.

$$\frac{\partial \rho}{\partial t} + \nabla \cdot [\rho \vec{v}] = 0 \tag{1}$$

$$\frac{\partial}{\partial t}(\rho \vec{v}) + \nabla \cdot [\rho \vec{v} \vec{v}] = \nabla \cdot [\mu \nabla \vec{v}] - \nabla p + S_M \tag{2}$$

$$\frac{\partial}{\partial t}(\rho c_p T) + \nabla \cdot [\rho c_p \vec{v} T] = \nabla \cdot [k \nabla T] + S_T \tag{3}$$

Where ρ is the density, $\vec{v}$ is the velocity vector, μ is the dynamic viscosity, p is pressure, C_p is the specific heat at constant pressure, T is the temperature, k is the thermal conductivity, S_T is the source term of energy, and S_M is the source term of momentum.

For the set of equations that model a compressible flow to be closed, it needs an equation of state to develop a relation between density, pressure, and temperature. Since, in the study, we analyzed R-134 fluid flows, we considered this fluid an ideal gas. Thus we used Sutherland's law, described in Equation 4, as the equation of state.

$$\mu = \mu_{ref} \left(\frac{T}{T_{ref}} \right)^{3/2} \frac{T_{ref} + S}{T + S} \tag{4}$$

Where T_{ref} is the reference temperature, μ_{ref} is the Dynamic viscosity at the reference temperature, and S is the Sutherland temperature.

2.2 Turbulence Model

Since the flow is assumed to be turbulent, we modeled it using the Reynolds-averaged Navier-Stokes equations (RANS). However, the equations need a turbulence model to be closed, as presented by Moukalled *et al.* (2016), and so, we need a model to compute the turbulent dynamic viscosity. The chosen model was the Spalart-Allmaras Turbulence Model (SA), its formulation presented by Rumsey (2014).

According to Rumsey (2014), the SA turbulence model is a one equation model in which the turbulent viscosity is computed as presented in the Equation 5.

$$\mu_t = \rho \nu_t \tag{5}$$

Being the turbulent kinematic viscosity ν_t is given Equation 6.

$$\nu_t = \tilde{\nu} f_{v1} \qquad f_{v1} = \frac{\chi^3}{\chi^3 + c_{v1}^3} \qquad \chi = \frac{\tilde{\nu}}{\nu} \tag{6}$$

The term $\tilde{\nu}$ introduced behaves like ν_t far from the wall ($y^+ > 30$), however, it has a linear behavior close to the wall, in the viscous sub-layer ($y^+ < 5$), while ν_t has a quadratic form in this region. Due to that, the variable f_{v_1} was added to approximate the shape of $\tilde{\nu}$ to ν_t close to the wall. The function f_{v_1} captures most of the viscous damping effects that happen on the viscous sub-layer. The one transport equation solved in this turbulence model is the transport equation for $\tilde{\nu}$ given Equation 7.

$$\frac{\partial \tilde{\nu}}{\partial t} + \nabla \cdot (\boldsymbol{U} \tilde{\nu}) = c_{b1} \bar{S} \tilde{\nu} + \frac{1}{\sigma} \left[\nabla \cdot (\nu + \tilde{\nu}) \nabla \tilde{\nu} + c_{b2} (\nabla \tilde{\nu})^2 \right] - c_{w1} f_w \left(\frac{\tilde{\nu}}{d} \right)^2 \tag{7}$$

The terms c_{b1}, c_{b2}, and c_{w1} are the constants of the SA turbulence model, being their values presented in Rumsey (2014). The variable S is the shear rate tensor, defined in Equation 8.

$$\boldsymbol{S} = \frac{1}{2} \left(\nabla \boldsymbol{U} + (\nabla \boldsymbol{U})^T \right) \tag{8}$$

3. METHODOLOGY

3.1 Geometry

During the study, the geometry used was the Benchmark Supercritical Wing (BSCW). This wing model was chosen for the AePW-2 because it has simple geometry and complex fluid flow. It was originally designed for the Benchmark Aeroelastic Models Program described in Bennett *et al.* (1991). This program was part of the efforts of the NASA Langley Research Center to provide the necessary data to evaluate CFD codes for aeroelastic analysis. Table 2 describes the geometric parameters of this wing.

Table 2. BSCW Geometrical parameters from Heeg *et al.* (2015).

Description	**Symbol**	**Value**
Reference chord	c_{ref}	0.4064 [m]
Model span	b	0.8128 [m]
Area	A	0.3303 [m^2]
Moment reference point relative to axis system def.	x	0.12192 [m]
	y	0.0000 [m]
	z	0.0000 [m]
Frequency Response Function reference quantity	FRF	Pitch angle

The wing section profile of the BSCW is a NASA SC(2)-0414, and the wing has a rectangular planform, both shown in Figure 1. The model was mounted to a large splitter plate, approximately 1 m away from the wall, the reasons being to keep the wing outside of the tunnel boundary layer and to place it closer to the tunnel centerline.

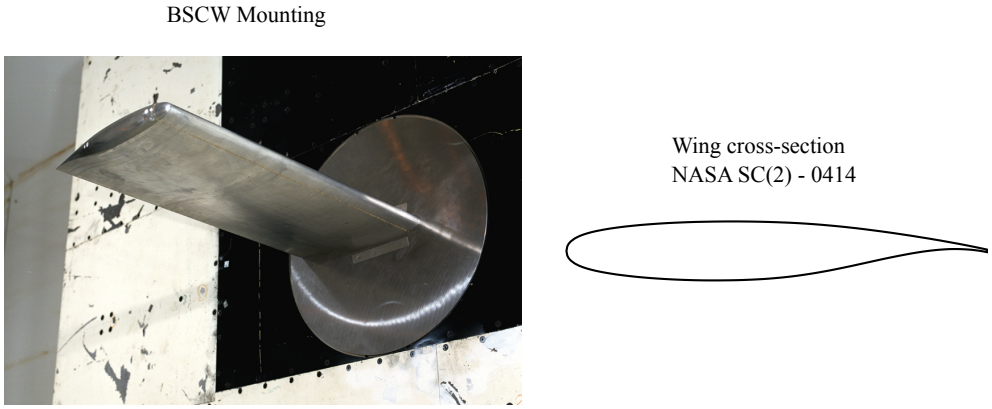

Figure 1. BSCW Tunnel Mounting System and Cross Section. Heeg *et al.* (2015)

This wing model can support having two chordwise rows of 40 in-situ unsteady pressure ports at the 60% and 95% span locations, with 22 ports on the upper surface, 17 ports on the lower surface, and 1 port at the leading edge for each row. However, for the forced oscillation tests, only the inboard row at the 60% span station was fully populated. The Oscillating Turntable (OTT) equipment was extensively tested by Piatak and Cleckner (2003).

3.2 Flow Conditions

In test case 3B, the BSCW was tested on the Oscillating Turntable (OTT) and the data was acquired for R-134a, Mach number of 0.85, and angle of attack of 5 degrees. To simulate the dynamic condition the wing oscillated in pitch at about 30% of the chord over with frequencies of 10 Hz. The Reynolds number was fixed at 4.56 million based on the wing chord. Other important flow conditions and input parameters are summarized in Table 3.

Table 3. Flow Properties from Heeg *et al.* (2015).

Property	**Freestream Velocity**	**Speed of sound**	**Temperature**	**Density**	**Sutherland Constant**	**Reference dynamic viscosity**	**Reference Temperature**
	$[m/s]$	$[m/s]$	$[K]$	$[kg/m^3]$	$[K]$	$[Ns/m^2]$	$[K]$
Symbol	V	c	T	ρ	C	μ_{ref}	T_{ref}
Value	118.058	168.655	304.2128	1.175	243.372	$1.11 \cdot 10^{-5}$	273

3.3 Mesh

One of the biggest challenges in using the SU2 solver is that it has no meshing capabilities and only supports meshes in CGNS or SU2 formats. The software chosen to generate the mesh was Salome version 9.7 [1]. Even though Salome can export meshes in `.cgns`, they were not accepted by the SU2 solver, then we used a third-party plugin called `cfdmsh` [2].

Salome has many meshing algorithms, but the one found to be the most reliable and presented better results was NetGen. A total of three meshes were created to evaluate the discretization error using the methodology described by Celik *et al.* (2008), in this methodology we create meshes with refinement increasing in a ratio of 1.3 and then compare the results for each mesh as presented in Section 4.1, Table 5 and Figure 3.

The parameters used to create the viscous layers in all of the three meshes were: Total thickness of $7.29019x10^{-4}$; 35 layers; stretch factor of 1.2. The domain was chosen with a diameter of $200c_{ref}$, as shown in Figure 2, along with the indication of the patches in which the boundary conditions were applied.

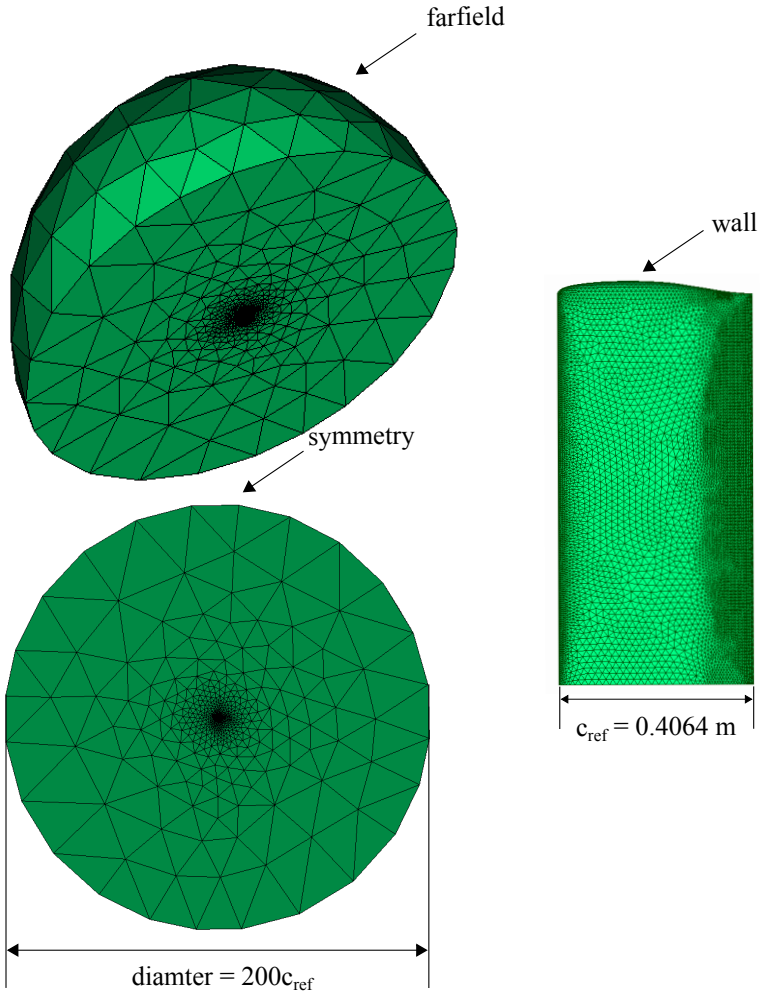

Figure 2. Mesh Generated in Salome.

3.4 Case Setup

Following the indication in Figure 2, Table 4 shows which boundary conditions were applied for each mesh patch.

Table 4. Boundary Conditions Employed.

Patch	wall	symmetry	farfield
Boundary Condition	noSlip	symmetry	farfield

[1] https://www.salome-platform.org/
[2] https://github.com/tougeron-cfd/cfdmsh

For the numerical setup Green-Gauss was used to compute the gradient; FGMRES with ILU preconditioner to solve the linear system; JST as the flow convective numerical method and Scalar Upwind as the turbulent convective numerical method. For the unsteady case, a Dual Time Stepping algorithm with second-order accuracy was employed to solve the time marching.

The post-processing application used was ParaView 5.10.1. More information about this tool can be found on [3].

4. RESULTS AND DISCUSSION

4.1 Static Analysis

Static analysis was performed to get a Grid Convergence Index. The procedure used was described by Celik *et al.* (2008). Table 5 shows the data obtained from the grid convergence analysis.

Table 5. Grid Convergence Index Analysis Developed.

$\mathbf{N_1, N_2, N_3}$	5392371 , 3054273, 1671187
Refinement factor $\mathbf{r_{21}}$	1.3287
Refinement factor $\mathbf{r_{32}}$	1.3519
Approximate relative error $\mathbf{e_{a21}}$	3.2%
Approximate relative error $\mathbf{e_{a32}}$	9.7%
Extrapolated relative error $\mathbf{e_{ex21}}$	1.7%
Extrapolated relative error $\mathbf{e_{ex32}}$	5.1%
Convergence index $\mathbf{GCI_{21}}$	2.2%
Convergence index $\mathbf{GCI_{32}}$	6.11%

In Table 5 the subindex represents the mesh, being 1 for coarse, 2 for medium and 3 for fine, the double subindex represents comparison of two meshes. N_{index} represents the number of elements in each mesh. Table 5 shows that the results for this test configuration are highly dependent on mesh refinement, once that the approximate relative error between meshes (e_{a32}) is more than three times the approximate relative error between the fine and the medium mesh (e_{a21}), which agrees with other studies, such as Begnini *et al.* (2016) and Raveh *et al.* (2018).

A comparison of the pressure coefficient among the three meshes tested and the experimental data provided by the workshop are presented in Figure 3. Given the GCI_{21} of 2.2%, mesh convergence was achieved between the fine and the medium mesh, this information is complemented in Figure 3 which shows similar results for meshes medium and fine. At Mach 0.85 the BSCW was found to have a moving shock wave Begnini *et al.* (2016), due to that the primitive variables do not tend to reach a constant value. For a direct comparison of the results with the experimental data, an unsteady analysis should be performed. The difficulty regarding the convergence of this case in a steady-state analysis was detailed in the overview paper for the first AePW by by Heeg (2013).

Due to limited computer resources and the mesh convergence achieved in the static analysis, only the medium mesh will be used for te forced oscillation analysis.

[3] https://www.paraview.org/

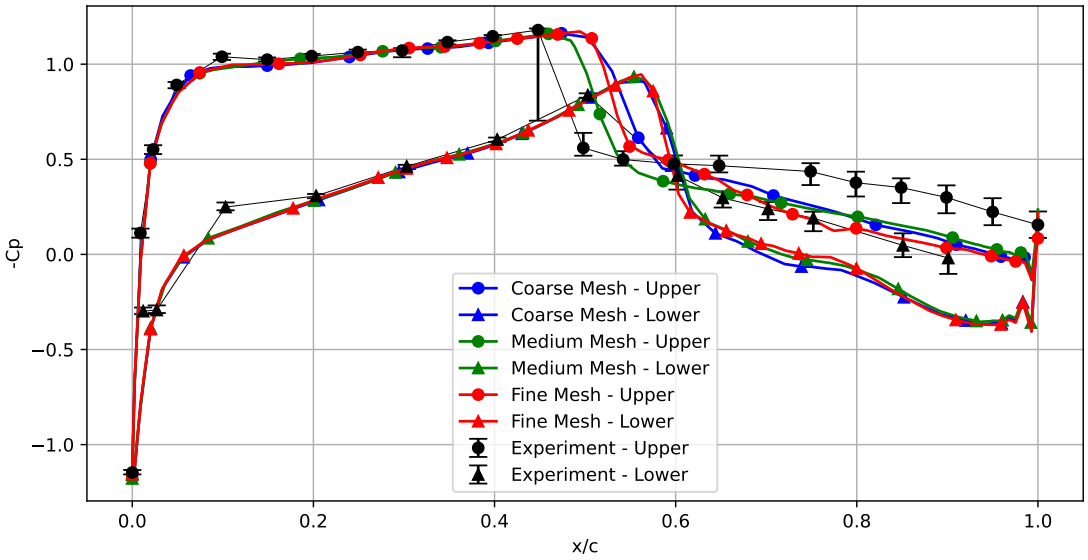

Figure 3. Results of the Static Analysis, Mach 0.85, AOA 5°.

The results in Figure 3 show that, before the shock region, there is a good agreement with experimental data. Even though the discontinuity caused by the shock was captured, the pressure recovery that occurs after it was not well represented. These results are very similar to those obtained by other authors in the literature, as summarized by Heeg *et al.* (2016).

As can be seen in Figure 3, our results presented some oscillations in the form of small peaks in the region after the shock, which diverges from the other studies found in the literature. These oscillations and the pressure recovery aren't being properly computed due to the poor quality elements and the low refinement of the mesh in the trailing edge region. The SA turbulence model employed may also not have been able to predict the detached flow induced by the shock wave, a phenomenon that was verified in the experiments, as pointed out by Heeg *et al.* (2015). Figure 4, shows the flow around the wing for the static analysis with the medium mesh. The shock waves on the upper and lower surface of the wing are visible in Figure 4. This figure also shows that for the static analysis, no detachment was captured.

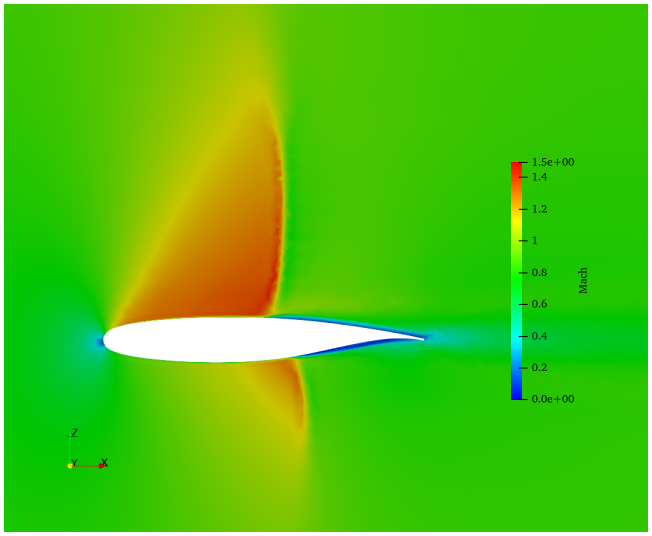

Figure 4. Mach filed for the Static Analysis, Mach 0.85, AOA 5°, Wing section at 60% of the span.

As a whole, the static analysis presented showed good agreement with other results from the literature and with experimental data. And so, proving that SU2 and Salome can be used to provide accurate numerical data even for complex flows in the transonic regime.

4.2 Forced oscillation

For case 3B, the wing oscillated in pitch with a frequency of 10 Hz and amplitude of 1°. The simulation was performed with the SA turbulence model using a physical time step of 10^{-3}s (100 time steps per cycle). Snapshots of the flowfield were taken at every time step and used to compute the Frequency Response Function (FRF) of the pressure coefficient C_P.

Figures 5 and 6 show the transfer function between the pressure coefficient and the pitch motion applied, respectively for the upper and lower surfaces of the wing, being the results presented in the figures compared with the experimental data provided by the AePW-2 in Heeg *et al.* (2015).

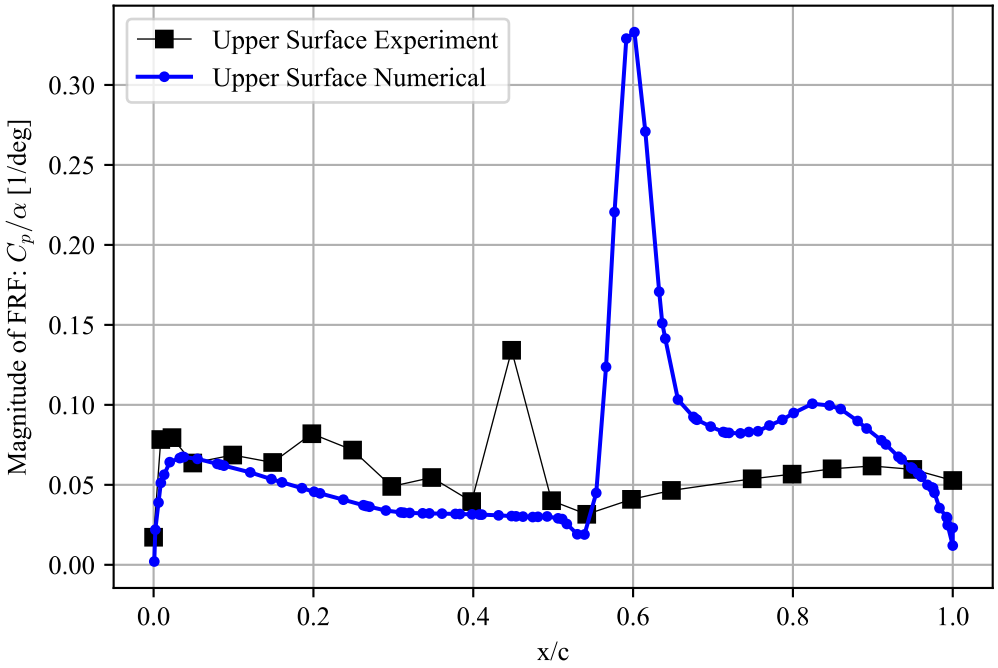

Figure 5. Magnitude of the transfer function, upper surface, with Mach 0.85, and 5° AOA.

The overall results for the upper surface are in line with those obtained by other authors, given that none of the results summarized in Heeg *et al.* (2016) were able to match the experimental data with high precision. However, the peak shown in Figure 5, at around 60% of the chord was not as overpredicted as ours was when compared to the results presented in Heeg *et al.* (2016) or in Raveh *et al.* (2018). Furthermore, the results in Figure 6 are also compatible with other numerical results such as the one presented by Raveh *et al.* (2018). Except that Raveh *et al.* (2018) could predict a peak next to 10% of the chord that was not captured in our results. Begnini *et al.* (2016) and Raveh *et al.* (2018) could predict the peaks with lower intensity for the magnitude of FRF but the general behavior of the transfer function was similar to those presented in Figure 5 and 6.

Raveh *et al.* (2018) argued that the fewer pressure ports in the lower surface could not have provided enough resolution to capture that shock, being this hypothesis complemented by the fact that the static analysis data shows a shock in the lower surface, see figures 3 and 4.

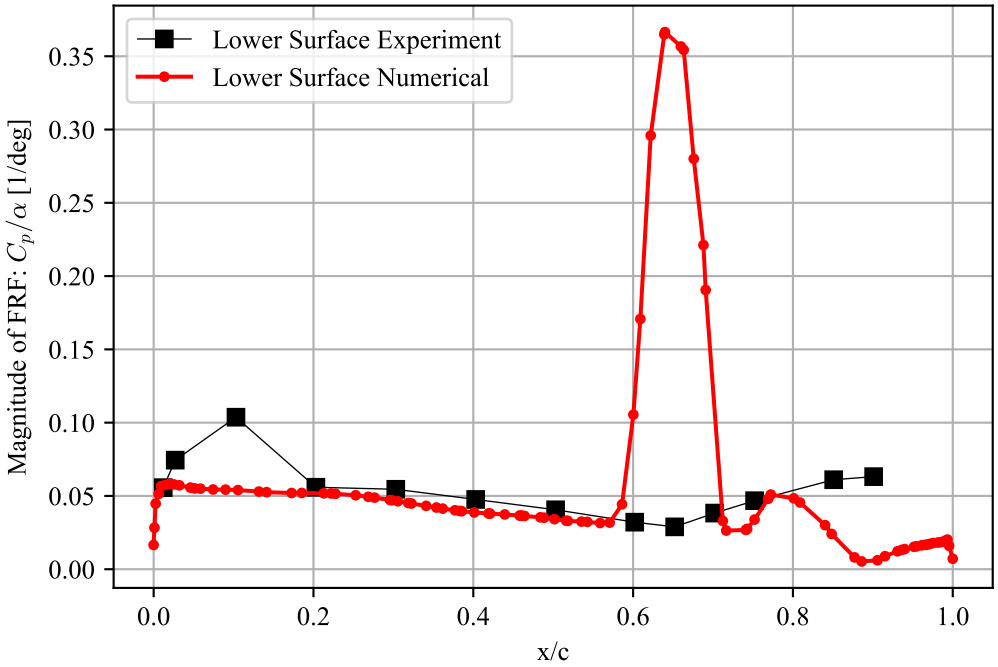

Figure 6. Magnitude of the transfer function, lower surface, with Mach 0.85, and 5° AOA.

5. CONCLUSIONS

During this study, we performed numerical simulations with the SU2 solver for case 3B of the second Aeroelastic Prediction Workshop. This case had a Mach number of 0.85 and an angle of attack of 5°, the simulations predicted with good accuracy the steady pressure distribution until the shock, moreover the SA turbulence model applied could not accurately predict the pressure recovery after the shock.

The response to prescribed pitch oscillations at 10 Hz and 1° pitch amplitude were not accurately predicted. However, the results showed the same trends found in other studies. The unsteady response may have diverged from the experiments due to a too sparse pressure measurement on the experiments, as pointed out by Raveh *et al.* (2018). Along with that, the mesh refinement plays a big role in the amplitude of the shock predicted, as our mesh was less refined than those used by other workshop participants, which could be the reason why we predicted a magnitude of approximately 0.35 and other authors predicted values of 0.15 to 0.25, for both surfaces.

With all the analyses, we confirmed the capability of SU2 to solve transonic problems and the capability of Salome to generate meshes for SU2 and CFD in general. Nonetheless, as the meshing algorithms used in Salome were not developed for CFD applications, it is difficult to get a high-quality mesh, mainly for more complex geometries.

6. ACKNOWLEDGEMENTS

This research was supported by resources supplied by the Center for Scientific Computing (NCC/GridUNESP) of the São Paulo State University (UNESP).

7. REFERENCES

Ballmann, J., Boucke, A., Chen, B., Reimer, L., Reimer, L., Behr, M., Behr, M., Dafnis, A., Buxel, C., Buesing, S. *et al.*, 2011. "Aero-structural wind tunnel experiments with elastic wing models at high reynolds numbers (hirenasd-asdmad)". In *49th AIAA Aerospace Sciences Meeting Including the New Horizons Forum and Aerospace Exposition*. p. 882.

Ballmann, J., 2008. "Experimental analysis of high reynolds number structural dynamics in etw". In *46th AIAA Aerospace Sciences Meeting and Exhibit*. p. 841.

Begnini, G.R., Spode, C., Pantaleao, A.V., Guaraldo, B., Marcório, G.D., Pedras, M.H. and Bones, C.A., 2016. "A comparison of CFD and AIC-Based methods for unsteady aerodynamics and flutter computations of the AePW-2 wing model". In *34th AIAA Applied Aerodynamics Conference*. p. 3123.

Bennett, R.M., Eckstrom, C.V., Jr, J.A.R., Dansberry, B.E., Farmer, M.G., and Durham., M.H., 1991. "The benchmark aeroelastic models program: Description and highlights of initial results."

Bisplinghoff, R.L., Ashley, H. and Halfman, R.L., 2013. *Aeroelasticity*. Courier Corporation.

Campos, H.M., Lazzarini, F.A.S. and Pantaleão, A.V., 2021. "Solution of AePW-2 test cases using open-source code". *International Journal of Advanced Engineering Research and Science*, Vol. 8, p. 6.

Celik, I.B., Ghia, U., Roache, P.J. and Freitas, C.J., 2008. "Procedure for estimation and reporting of uncertainty due to discretization in CFD applications". *Journal of fluids Engineering-Transactions of the ASME*, Vol. 130, No. 7.

Chwalowski, P., Florance, J., Heeg, J., Wiseman, C. and Perry, B., 2011. "Preliminary computational results of hirenasd configuration in preparation for the aeroelastic prediction workshop". *IFASD_2011-108, June*.

Economon, T.D., Palacios, F., Copeland, S.R., Lukaczyk, T.W. and Alonso, J.J., 2016. "SU2: An open-source suite for multiphysics simulation and design". *AIAA Journal*, Vol. 54, No. 3, pp. 828–846.

Heeg, J., 2013. "Overview of the aeroelastic prediction workshop". In *51st AIAA aerospace sciences meeting including the new horizons forum and aerospace exposition*. p. 783.

Heeg, J., Chwalowski, P., Raveh, D.E., Dalenbring, M.J. and Jirasek, A., 2015. "Plans and example results for the 2nd AIAA aeroelastic prediction workshop". In *56th AIAA/ASCE/AHS/ASC Structures, Structural Dynamics, and Materials Conference*. p. 0437.

Heeg, J. and Piatak, D.J., 2013. "Experimental data from the benchmark supercritical wing wind tunnel test on an oscillating turntable". In *54th AIAA/ASME/ASCE/AHS/ASC Structures, Structural Dynamics, and Materials Conference*. p. 1802.

Heeg, J., Wieseman, C.D. and Chwalowski, P., 2016. "Data comparisons and summary of the second aeroelastic prediction workshop". Technical report.

Moukalled, F., Mangani, L., Darwish, M. *et al.*, 2016. *The finite volume method in computational fluid dynamics*, Vol. 113. Springer.

Palacios, F., Economon, T.D., Aranake, A., Copeland, S.R., Lonkar, A.K., Lukaczyk, T.W., Manosalvas, D.E., Naik, K.R., Padron, S., Tracey, B., Variyar, A. and Alonso, J.J., 2014. "Stanford university unstructured (SU2): Analysis and design technology for turbulent flows". In *52nd Aerospace Sciences Meeting*. American Institute of Aeronautics and Astronautics.

Piatak, D.J. and Cleckner, C.S., 2003. "Oscillating turntable for the measurement of unsteady aerodynamic phenomena". *Journal of aircraft*, Vol. 40, No. 1, pp. 181–188.

Raveh, D.E., Mor Yossef, Y. and Levy, Y., 2018. "Analyses for the second aeroelastic prediction workshop using the EZNSS code". *AIAA Journal*, Vol. 56, No. 1, pp. 387–402.

Rumsey, C., 2014. "The Spalart-Allmaras turbulence model". *Turbulence Modeling Resource.[Online]. Available: https://turbmodels. larc. nasa. gov/spalart. html.[Accessed: 05-May-2017]*.

Sanchez, R., Kline, H., Thomas, D., Variyar, A., Righi, M., Economon, T.D., Alonso, J.J., Palacios, R., Dimitriadis, G. and Terrapon, V., 2016. "Assessment of the fluid-structure interaction capabilities for aeronautical applications of the open-source solver SU2".

8. RESPONSIBILITY NOTICE

The authors are solely responsible for the printed material included in this paper.